Geophys. J. Int. (2006) **165,** 705–718 doi: 10.1111/j.1365-246X.2006.02923.x

Joint inversion of gravity and geoelectrical data for groundwater and structural investigation: application to the northwestern part of Sinai, Egypt

F. A. Monteiro Santos,[1] S. A. Sultan,[2] Patrícia Represas[1] and A. L. El Sorady[3]

[1] *Universidade de Lisboa and Centro de Geofísica da Universidade de Lisboa (CGUL), Campo Grande, Ed.* C8, 1749-016 *Lisboa, Portugal. E-mail: fasantos@fc.ul.pt*

[2] *National Research Institute of Astronomy and Geophysics (NRIAG), Helwan, Cairo, Egypt*

[3] *Geological Survey of Egypt, Cairo, Egypt*

Accepted 2006 January 17. Received 2005 December 19; in original form 2005 May 27

SUMMARY

The simulated annealing method was applied to jointly invert gravity and resistivity data to obtain the geometry of the density/resistivity interfaces and subsurface electrical resistivity distribution. The results obtained from the inversions of synthetic data indicate that the joint inversion significantly improves the solution decreasing the ambiguity of the models. The method was applied to gravity and resistivity data carried out in Sinai (northwestern Egypt). The results obtained revealed the geometry of the water-bearing zone with thickness ranging from 80 to 180 m and of the limestone–bedrock interface dipping northwards.

Key words: Egypt, electrical resistivity, gravity, groundwater, inversion, tectonics.

1 INTRODUCTION

Gravity and resistivity are two methods that play major roles in tectonic studies, mineral explorations and in environmental and engineering problems (Parasnis 1986; Telford *et al.* 1978). However, both methods present limitations in resolving model parameters. The non-uniqueness in the density distribution and depth of the interfaces obtained from inversion of gravity data is well known (e.g. Li & Oldenburg 1998; Blakely 1995). Since the gravity field is only measured on the surface of the Earth, there is an infinite number of equivalent density distributions that will fit the measured gravity values equally well. In the inversion of resistivity data acquired in layered or gently dipping geology, the equivalence and suppression problems are also well known (Parasnis 1986).

The limitations and ambiguity of individual techniques can be significantly reduced by adopting joint inversion schemes. Different measured quantities can be integrated into a joint inversion if the measured data are influenced by a subset of common subsurface parameters. In some particular environments, a relationship between these parameters is explicitly stated. However, there are special techniques that allow the joint inversion even if such an explicit relationship does not exist or is not known (Haber & Oldenburg 1997; Gallardo & Meju 2004). In a joint inversion scheme all the data set is simultaneously inverted and a unique model is estimated.

There are several works dealing with joint inversion methods of different data. When combining resistivity, magnetotelluric and transient electromagnetic (TDEM) data in a joint inversion procedure (Vozoff & Jupp 1975; Meju 1996; Harinarayana 1999), all the data are sensitive to the same resistivity model. In the joint inversion of seismic and resistivity data acquired over a layered earth the layer thickness is the only common parameter (Kis 2002). In this case layer interfaces are assumed to be the same for both geoelectrical and seismic properties in order to perform the joint inversion.

The bulk density σ_e and fractional porosity ϕ, of porous media partially filled with water is just the volume weighted density expressed by:

$$\sigma_e = (1-\phi)\sigma_m + S_w\phi\sigma_w, \tag{1}$$

where σ_m is the rock matrix density and σ_w the pore-water density, and S_w is the fractional amount of saturation of pore water. The effect of the air in the pores is not considered in this equation. Connection between bulk density and resistivity of a geological formation can be done through the porosity, using the Archie's law. For clay-cleaned rocks and low-frequency or DC methods the Archie's law is expressed by (Grant & West 1965),

$$\rho_e = a\rho_w S_w^{-n}\phi^{-m}, \tag{2}$$

where a, n and m are empirical constants, ρ_w and ρ_e are the water and the bulk resistivity, respectively. Combining eqs (1) and (2) the bulk density will be expressed by,

$$\sigma_e = (1-\phi)\sigma_m + \left[a\rho_w/\left(\rho_e\phi^{m-n}\right)\right]^{1/n}\sigma_w. \tag{3}$$

According to eq. (3) it is possible to have several different combinations of porosity, bulk and water resistivity and matrix density that fit the data equally well. This is the expression of the known problem of non-uniqueness solution in gravity. If $n = m$, a frequently adopted condition, eq. (3) is expressed by

$$\sigma_e = (1-\phi)\sigma_m + \left[a\rho_w/\rho_e\right]^{1/n}\sigma_w. \tag{4}$$

In this case, a linear relationship between bulk density and porosity is established. A more complex relationship between bulk density and bulk resistivity is also revealed. In this work it is assumed that the interfaces corresponding to changes in the bulk density are also interfaces of porosity and water content changes. Therefore, those interfaces are also associated to electrical resistivity changes.

An algorithm based on simulated annealing (SA) technique is proposed in this paper to jointly invert gravity and resistivity (Vertical Electrical Soundings, VES) data for the delineation of resistivity/density interfaces and electrical resistivity distribution. Taking into account the VES limitations in depth investigation only a few layer-interfaces positions will be considered as common parameters in this scheme. Resistivity values of the layers are also considered as parameters in this algorithm but a previous knowledge of the density distribution is assumed.

The program was tested using synthetic data. A field example from Egypt was chosen to exemplify the application to structural and groundwater resource studies.

2 JOINT INVERSION USING SIMULATED ANNEALING

Resistivity and gravity data inversion is a non-linear problem usually solved by applying Tikhonov-Occam method (e.g. Tikhonov & Arsenin 1977; DeGroot-Hedlin & Constable 1990; Sasaki 1989; Loke & Barker 1996; Li & Oldenburg 1998; Barbosa *et al.* 1999). When seeking for a density (or electrical resistivity) distribution, the subsurface zone of interest is divided into a large number of (rectangular) cells and the density contrast (or resistivity) of each cell is calculated minimizing an appropriate objective function.

The geometry of density-interfaces determination (in 2-D or 3-D approach) from gravity data is a classical problem. Several authors have presented different algorithms: Cordell & Hederson (1968) used rectangular prisms of constant density to model the perturbing body; Tsuboi (1983) proposed a method based on equivalent stratum technique to compute the interface; Oldenburg (1974) in order to determine the geometry of the density interface used the Fourier transform technique developed by Parker (1973). If the problem consists in determining the geometry of only one interface the solution is in general good (e.g. Bott 1960; Barbosa *et al.* 1999; Roy *et al.* 2002, among several others). The solution found using any of these methods is greatly improved if *a priori* constraints (e.g. from borehole logs) are introduced. However, the problem gets more difficult if more than one interface needs to be estimated. In this case additional information, generally from boreholes, is necessary. The method proposed here seeks to use information from VES instead of borehole data.

Vertical electrical soundings (or magnetotelluric soundings) are often used to determine the resistivity structure (i.e. the electrical resistivity distribution and the resistivity-interfaces geometry) of sedimentary environments. This is also a classical inverse problem, the solution of which was presented by several authors using stitched 1-D (e.g. Patra & Battacharya 1966; Koefoed 1979; Johansen 1977) or 2-D models (Dey & Morrison 1979; Smith *et al.* 1999; DeGroot-Hedlin & Constable 2004).

All the referred algorithms are called local optimizers and their performances depend on the proximity of the initial model to the 'real' solution. In the last years the interest in the application of global optimization techniques, for example, genetic algorithm (GA), controlled random search (CRS), SA, etc. to geophysical problems has been increasing and a better convergence to global minimum of the objective functions has been reported by several authors (Kirkpatrick *et al.* 1983; Rothman 1986; Dittmer & Szymansky 1995; Dosso & Oldenburg 1991; Sen & Stoffa 1995; Pessel & Gibert 2003).

The SA has this designation due to the analogy with the process of physical annealing in thermodynamics: the undetermined parameters of the geophysical model are analogue to the particles of the physical system. The objective function of the inverse problem is analogue to the energy of the physical system. Similar to the annealing process, which is controlled by initial temperature and cooling schedule, the estimation of the solution in the inverse problem is also controlled by a positive parameter T, which limits the perturbation of the parameters values that is acceptable. The acceptability of a change is based on the algorithm presented by Metropolis *et al.* (1953).

According to this algorithm, perturbations of the parameters conducive to a decrease in the objective function are systematically accepted. When an increase in the objective function is verified the changes in the parameters are not systematically rejected. Instead the acceptance of the new parameters depends on the value of the function (which represents an acceptance probability)

$$\Psi = \exp(-\Delta E / T), \tag{5}$$

(where ΔE represents the objective function variation), that is compared with a randomly generated number χ, between 0 and 1. The changes in the model are accepted if $\Psi > \chi$ and are rejected otherwise.

For high values of T (corresponding to high temperatures of a 'melted' physical system) virtually all changes are accepted. The Metropolis algorithm iterates over a sequence of models at a constant T value. This renders the solution independent of the initial model and allows the algorithm to escape from local minima. Looping over the Metropolis algorithm, while T decreases, it is expected that the accepted models will concentrate in the vicinity of the absolute minimum of the objective function, with the decrease in the acceptance probability (eq. 5) only perturbations decreasing the objective function are accepted. A slowly decreasing T parameter is important in the efficiency of the SA algorithm, allowing a representative sampling of the parameters space.

In order to apply the SA method, the subsurface is divided in rectangular cells as shown in Fig. 1 together with the measurement layout. The vertical dimension of the cells is limited by the position of the density/resistivity interfaces. The density of the cells between two interfaces is considered constant but the resistivity beneath each VES is allowed to vary. For a resistivity survey with VES carried out closely and showing lateral changes, the model resistivity values might be constrained to be laterally consistent. In this work the 1-D approach used in VES calculations and the option of not using lateral constraints, is justified by the similarity of the DC data and by the large spacing between VES sites (when compared with the depth of investigation of each sounding). The 2-D forward modelling, should be adopted if VES spacing is of the same order of the VES depth of investigation.

An objective function, E based on l_1-norm and involving gravity and resistivity data and smooth interfaces is defined as:

$$E = \varepsilon_1 E_g + \varepsilon_2 \sum_{p}^{P} E_{\mathrm{VESp}} + \lambda \sum_{k=1}^{K} S_k, \tag{6}$$

where P is the number of vertical electrical soundings, K is the number of interfaces in the model, ε_1, ε_2 and λ are weights whose values depend on relative importance of gravity, apparent resistivity

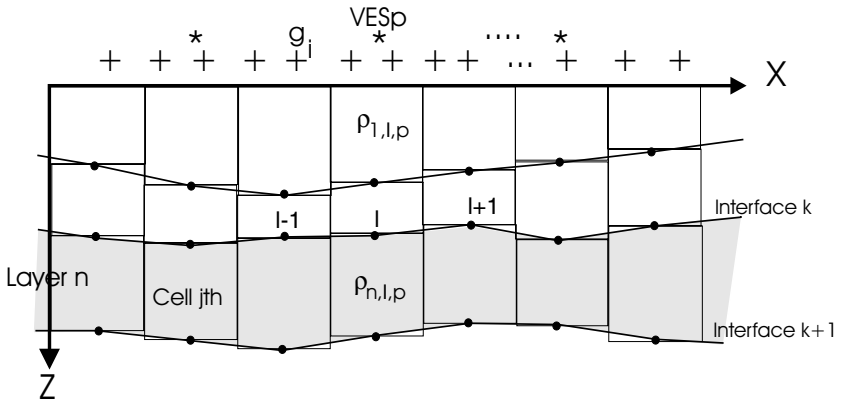

Figure 1. Model and layout of the surveys used in this work. The gravity data are acquired at sites marked '+' while the vertical electrical soundings are carried out at sites marked '*'. The density/resistivity interfaces are approached by the horizontal edges of the cells and represented by dots with coordinates (x_l, z_l). g_i is the ith gravity measurement; VESp is the pth electrical sounding. The nth layer is limited by interfaces k and $(k+1)$. Three points of the interface k are marked (points $l-1$, l and $l+1$, respectively). The resistivity of the cell l belonging to layer n and beneath VES p is represented by $\rho_{n,l,p}$.

data and the smoothness of the interfaces. E_g, E_{VESp} and S_k (the smooth of the kth interface) are defined as (see, Roy *et al.* 2002):

$$E_g = \frac{2\sum_{i=1}^{Ng}\left(\left|g_i^{\mathrm{obs}} - g_i^{\mathrm{cal}}\right|\right)}{\sum_{i=1}^{Ng}\left(\left|g_i^{\mathrm{obs}} - g_i^{\mathrm{cal}}\right|\right) + \sum_{i=1}^{Ng}\left(\left|g_i^{\mathrm{obs}} + g_i^{\mathrm{cal}}\right|\right)}, \tag{7i}$$

$$E_{\mathrm{VESp}} = \frac{2\sum_{i=1}^{\mathrm{Nvesp}}\left(\left|y_i^{\mathrm{obs}} - y_i^{\mathrm{cal}}\right|\right)}{\sum_{i=1}^{\mathrm{Nvesp}}\left(\left|y_i^{\mathrm{obs}} - y_i^{\mathrm{cal}}\right|\right) + \sum_{i=1}^{\mathrm{Nvesp}}\left(\left|y_i^{\mathrm{obs}} + y_i^{\mathrm{cal}}\right|\right)}, \tag{7ii}$$

$$S_k = \frac{1}{N_k}\frac{\sum_{l}^{N_k}\left(|z_{l-1} - 2z_l + z_{l+1}|\right)}{(x_{l+1} - x_{l-1})}. \tag{7iii}$$

The observed and calculated values are denoted by superscripts *obs* and *calc*, respectively. g stands for gravity values and y for the apparent resistivity in logarithmic domain. The subscripts p and k stand for the VES sounding pth and the kth interface, respectively. N_k is the number of segments in the kth interface, *Nvesp* is the number of apparent resistivity values in the pth electrical sounding and *Ng* is the number of gravity measurements. The meanings of z_l and of x_l and of the other symbols are evident from Fig. 1. The misfit between data and model response will be characterized by the relative error given by:

$$e = \frac{1}{N}\sqrt{\sum_{i}^{N}\left(\frac{d_i^{\mathrm{obs}} - d_i^{\mathrm{cal}}}{d_i^{\mathrm{obs}}}\right)^2}\, x100 \text{ per cent}, \tag{8}$$

where N is the total number of inverted data points and d represents the data set (gravity and apparent resistivity).

3 SYNTHETIC EXAMPLE

Data generation

Synthetic data generated from the model shown in Fig. 2 were used to test the reliability and accuracy of the algorithm. This model represents a frequent geological environment: a horst basement structure covered by layered sediments. It is also similar to the expectable structure in Sinai region. This model will allow us to understand the limitations of the method in the particular case study presented in this paper. The resistivity and density of each layer are summarized in Table 1. The VES were carried out at each 2 km totalizing nine

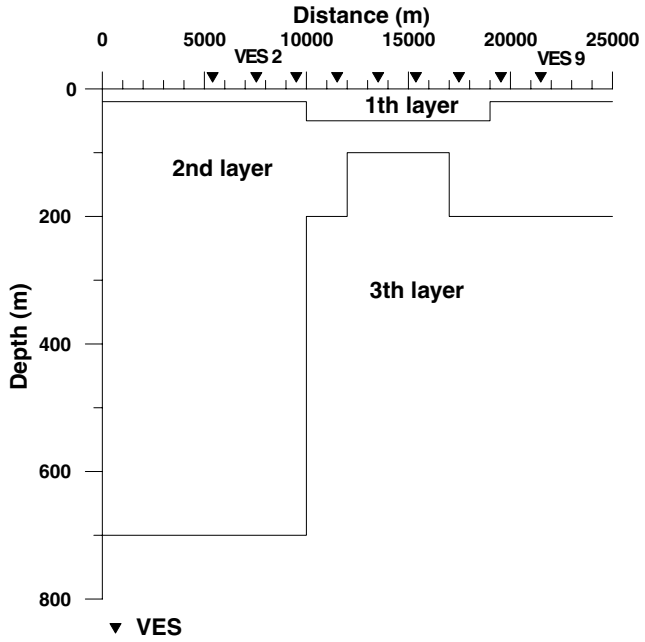

Figure 2. Model used for generation of the synthetic data (gravity and VES) shown in Figs 3 and 4. The model parameters are shown in Table 1. Note the exaggeration on the scale of the vertical axes.

soundings. At each VES site 21 values of apparent resistivity for AB/2 spacing ranging from 1.5 to 500 m were calculated assuming layered models (see, e.g. Koefoed 1979, for details about such calculations). The gravity data were calculated assuming 2-D models. Dividing the earth region of interest in small rectangular cells, the gravity effect at the ith data point is given by

$$g_i = \sum_{j}^{M} A_{ij}\sigma_j \qquad i = 1, \ldots\ldots Ng \tag{9}$$

where σ_j is the contrast density of the cell jth, A_{ij} represents the influence of the cell jth on the ith gravity value and M is the number of cells. The expression for A_{ij} can be found in, for example,

Table 1. Parameters used to generate synthetic data.

Layer	Density (kg m^{-3})	Resistivity (ohm-m)
1	2000	200
2	2150	4
3	2300	500

Last & Kubik (1983). The gravity values were calculated at each 1 km in a total of 21 values. Random data of 1 per cent of the average of absolute values of the data were added to each data set (Figs 3 and 4).

The depth of investigation of the VES is of about 200–250 m. It means that in a joint inversion of the gravity-VES data set only the interfaces located at a depth less than 250 m will be constrained by the resistivity data. The interfaces at a depth greater than 250 m will only be estimated from gravity data.

Separate inversion of synthetic data

The separate inversion of each data set was carried out in order to investigate the accuracy and reliability of the parameters estimated from each method and the benefits of the joint inversion. The accuracy of the parameter estimation is quantified by the relative parameter distance D_p given by:

$$D_p = \frac{1}{M}\sqrt{\sum_i^M \left(\frac{p_i^{\text{exact}} - p_i^{\text{cal}}}{p_i^{\text{exact}}}\right)^2}\, x\,100 \text{ per cent}, \qquad (10)$$

where p_i represents the ith value of the inverted parameter and M is the total number of values of the parameter. The parameters used in the separate inversion are: (1) the depth of the density contrasts in gravity data inversion and (2) the layer thickness and resistivity in VES inversion.

Fig. 3(a) shows the model obtained from the gravity data using a SA algorithm similar to the one presented here for joint inversion.

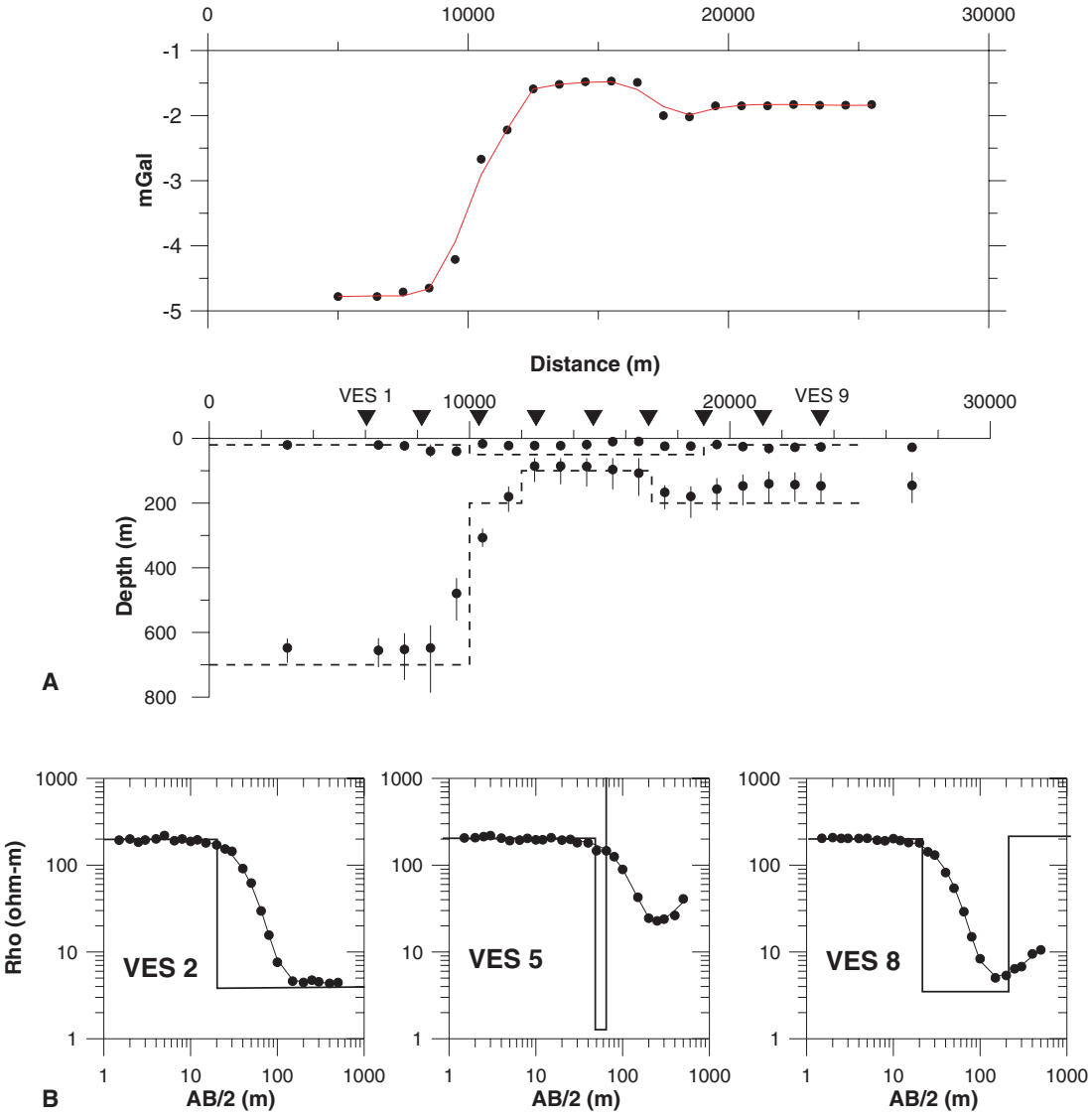

Figure 3. (a) Model obtained from the separate inversion of the gravity data shown in the upper part of the figure (dots). The average position of the interface is represented by dots while the vertical bars represent the maximum and minimum values of the interface position. The 'true' model is represented by dashed lines. (b) Results of the 1-D inversion of three representative VES data (symbols). The models are represented by thick lines and the model responses by thin lines.

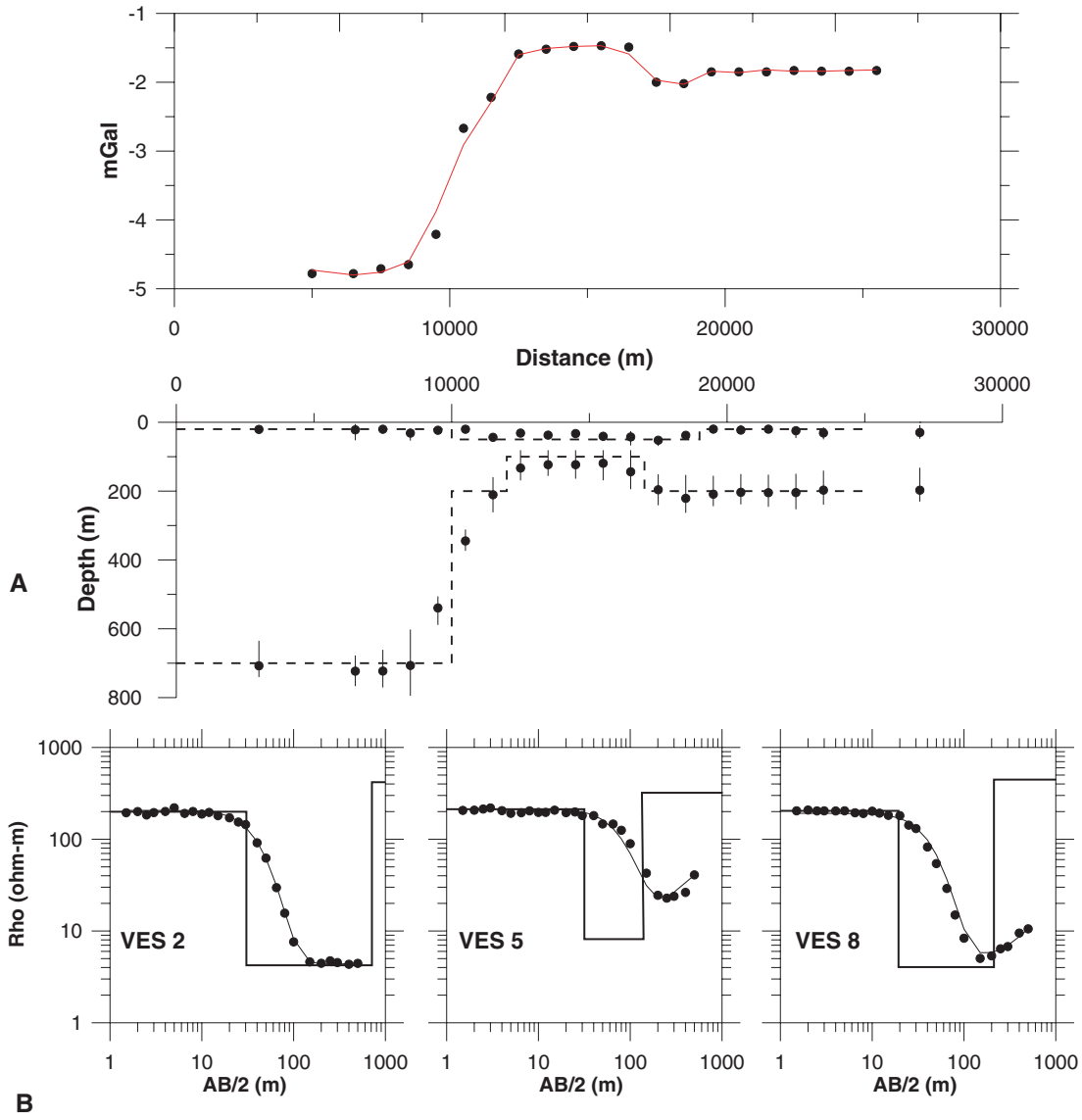

Figure 4. (a) Model obtained from the joint inversion of the gravity and VES data. The average position of the interface is represented by dots while the vertical bars represent the maximum and minimum values of the interface position. Gravity data (symbols) and model response (solid line) are shown in the top. (b) Comparison between VES data (symbols) and model responses (solid lines) for three representative sites.

The search limits for the interfaces depth are shown in Table 2. The result reveals that the uppermost interface is not well resolved ($D_1 = 12.5$ per cent), mainly in the zone corresponding to bedrock outcrop. The second density interface is also not well resolved ($D_2 =$ 40 per cent). The misfit is mainly observed in the deepest part of the interface.

Fig. 3(b) shows three representative VES together with the respective 1-D models obtained by inversion using layered models (Koefoed 1979). VES-2 carried out at site $x = 7500$ m does not sample the third layer. The thickness and resistivity of the first layer are well resolved, as well as the resistivity of the intermediate layer. The model obtained from VES-5 located at $x = 13\,500$ m does not resolve the intermediate and the last layers. In this case the intermediate layer is embedded between two more resistive layers and the obtained model is equivalent to any other for which the conductance of the second layer has approximately the same value ($S = h/\rho =$ 50/4 Siemens). The parameters of the two uppermost layers at the site of the VES-8 are quite well resolved by inverting the data. The deepest layer is, however, not well resolved.

Table 2. Search limits used in the SA inversions of the synthetic data.

Parameter	Max.	Min.
z_1	60 m	5 m
z_2	1000 m	61 m
r_1	600 ohm-m	10 ohm-m
r_2	20 ohm-m	1 ohm-m
r_3	1700 ohm-m	200 ohm-m

Joint inversion of synthetic data

The joint gravity–resistivity SA inversion was carried out with a starting parameter T of 0.5 and a cooling scheme of the type $T_n = 0.99\,T_{n-1}$, where n is the iteration number. The values of the parameters ε_1, ε_2 and λ were 0.45, 0.55 and 1.3, respectively. These

Table 3. Averaged resistivity (in bold) and its maximum and minimum values (calculated over six models) of the layers beneath each VES. Values in ohm-m. The models were estimated from joint inversion of gravity and resistivity synthetic data.

	VES-1	VES-2	VES-3	VES-4	VES-5	VES-6	VES-7	VES-8	VES-9
1st	**201.5**	**200.4**	**193.4**	**210.3**	**207.7**	**210.6**	**193.4**	**207.7**	**199.7**
layer	217.4	214.5	216.7	223.0	222.7	226.9	210.8	220.8	213.6
	188.3	190.2	177.1	197.8	193.	202.2	178.3	191.3	191.3
2nd	**4.0**	**4.1**	**3.8**	**5.1**	**8.4**	**7.1**	**4.0**	**4.0**	**4.0**
layer	4.3	4.6	4.2	7.6	12.0	12.7	6.0	4.7	4.9
	3.6	3.6	3.4	2.5	5.1	3.3	2.6	2.9	3.3
3rd	**418.4**	**434.8**	**410.5**	**372.1**	**318.5**	**745.7**	**451.2**	**463.1**	**404.5**
layer	647.8	693.6	700.0	933.1	632.1	1213.9	721.7	960.9	834.1
	200.0	202.5	213.6	209.8	200.0	454.0	200.0	200.0	221.2

values were obtained after several tests. For the SA inversion the used search limits of each parameter are given in Table 2.

Fig. 4(a) shows the models obtained from six runs of the SA algorithm. Fig. 4(b) shows the comparison between input synthetic data (symbols) and model responses (lines) obtained in one of the inversions run. The value of the objective function is 0.04 and the misfits for gravity and VES data are 0.7 and 6.6 per cent, respectively. The resistivity distribution beneath each VES site is displayed in Table 3. The overall model is quite well recovered; the geometry of the interfaces is well recovered ($D_1 = 6.6$ per cent and $D_2 = 4.5$ per cent). The large and the small steps at coordinates $x = 10$ km and $x = 17$ km are quite well defined. The resistivity of the first layer (beneath the VES sites) is also well resolved $D_\rho = 2.0$ per cent. The resistivity of the second layer is in general well recovered. However, at sites 4, 5 and 6 the equivalence phenomenon (allowing only the determination of the second layer conductance) makes the estimation of the resistivity inaccurate ($D_\rho = 24.4$ per cent). That phenomenon is, therefore, mainly responsible for the misfit of the interfaces geometry observed beneath those sites. As in the separate inversion, the resistivity of the last layer is quite well resolved at sites 1, 2, 3, 7, 8 and 9 but not at sites 4, 5 and 6.

The presented results revealed that the joint inversion of gravity and resistivity data makes possible the modelling of intermediate density interfaces improving the accuracy and reliability of the model parameters estimation.

4 APPLICATION TO SINAI DATABASE

The inversion method described above was applied to a data set acquired in Egypt. The study area is located at the northwestern corner of Sinai and is bounded by latitudes 30° 45′ and 31° 15′N and longitudes 32° 20′ and 33° 10′ E (Fig. 5). This part of Egypt is covered by sand dunes and is inhabited by Bedouins suffering from the scarcity of water necessary for domestic use.

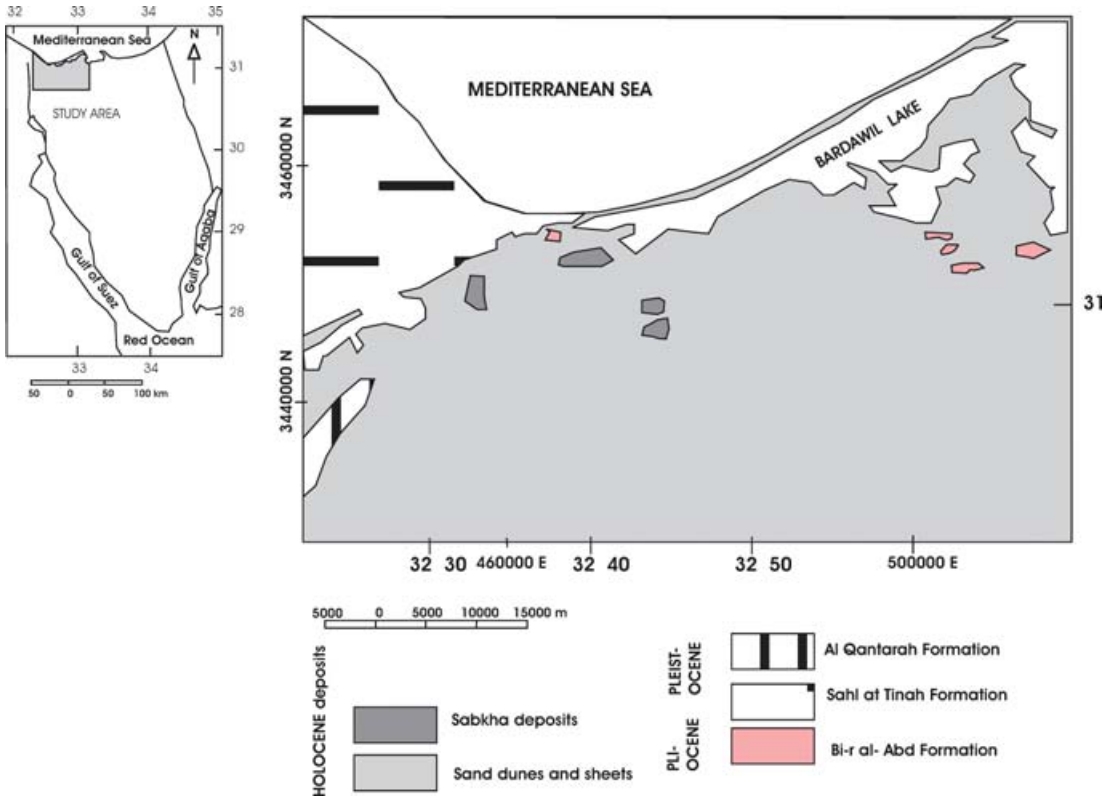

Figure 5. Location of the study area in Egypt and general geology overview.

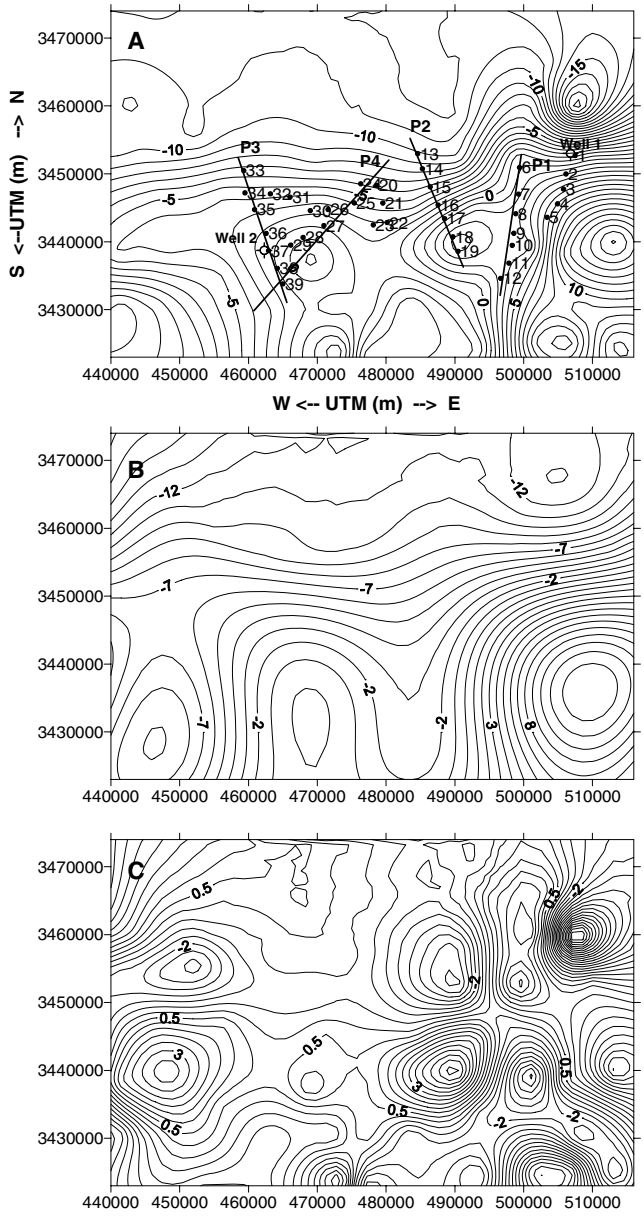

Figure 6. (a) Bouguer anomaly map and VES location. (b) Regional anomaly map obtained by filtering the Bouguer map using a low-pass filter defined in the wavenumber domain. (C) Residual anomaly map. Contours are in mGal (1 mGal $= 10^{-5}$ ms^{-2}).

Geoelectrical and gravity measurements were carried out in the area in order to detect water-bearing zones and shallow structural elements that affected the geometry of the groundwater aquifers (Sultan & El Sorady 2001). 39 vertical electrical soundings were measured to define different geoelectrical units, geometry of the water-bearing zones and groundwater quality (Fig. 6a). The soundings were roughly arranged along profiles extending mostly N–S in order to cover the northwestern part of Sinai. All measurements were taken with current electrode spacing ranging from AB/2 = 1.5 m to 500 m and using a Russian Electronic Compensator, type AE-72.

131 gravity stations were measured covering the study area. Gravity data were carried out to detect the shallow structural elements, which control the presence of groundwater. The gravity measurements were taken using the CG-3 Autograv (Sintrex) with resolution of 0.01 MGal. Different corrections were deduced using specialized Geosoft Programs (1994) such as drift, tide, latitude, free air, Bouguer and topographic corrections. The Bouguer anomaly map is shown in Fig. 6(a). The map shows different gravity gradients with ENE–WSW, N–S and NW–SE trends. The northern part of the survey area is characterized by low- gravity values(−19 mGal) and the southwestern has high values (16 mGal).

Geology of the area

The geological map of the study area shows different geological units of different ages (Fig. 5). The Holocene facies is composed of sabkha deposits as pockets south of Bardawil Lake; sand dunes and sand sheets cover most of the study area. The Pleistocene deposits are represented by Al-Qantarah Formation, which is composed of sand and grits with minor clay interbeds and Sahl Attina Formation, which is composed of mixture of black and white sands and silts. The Pliocene deposits are represented by Bir El-Abd Formation, which consists of shale intercalated with marl and fossiliferous limestone.

The shallow subsurface stratigraphy as shown by Bir El-Abd borehole consists mainly of clastic rocks such as loose sand, porous sand having water of salinity ranging from 2000 to 4000 ppm, sand clay having saline water (7000–9000 ppm) and clay and sands of Pleistocene age. However, marly limestone is present at 220 m. The water level depth in the borehole was 18 m.

Previous interpretation

The regional anomaly values (Fig. 6b), obtained by filtering the Bouguer anomaly map, suggest that the basement complex is shallower at the southeastern and southwestern parts of the area and become deeper northwards. The most prominent fault trend ENE–WSW is shown in this map along the middle zone.

The residual anomaly map (Fig. 6c) indicates different trends of the structural elements such as the ENE–WSW one located at the northern part of the survey. This structure shows a downthrow to the north direction that represents the Pelusium fault parallel to the Syrian Arc system. NW–SE trends are displayed at the southwestern and southeastern parts while NE–SW trends are visible at the eastern and northwestern regions. A N–S trend is also noted at the southern part of the study area.

The vertical electrical soundings were interpreted by Sultan & El Sorady (2001) using the Program (1993). The results of the interpretation were correlated with the data log from two boreholes drilled close to soundings VES-1 and VES-37 (Fig. 7). The results revealed the existence of three major resistivity layers. The first layer is characterized by relative high-resistivity values (100–5000 ohm-m) and thickness varying from 3.5 to 39 m correlating with dry sands. The second layer presents relative low-resistivity values (2–12 ohm-m) due to the water bearing with different water salinity and thickness ranging from 30 to 120 m. The third layer is characterized by very low-resistivity values (0.5–2 ohm-m) due to the saline groundwater intrusion from the Mediterranean Sea. Lithologically, this layer consists of silt and silty sand that may be of old Nile Province and also contains saline water at depths ranging from 30 to 150 m. In general the VES soundings did not give information about the marly limestone formation. It should be noted that in general the equivalence phenomena will be absent because the apparent resistivity curves are of the type Q and DH (i.e. $\rho_1 > \rho_2 > \rho_3$). Nevertheless, the bottom of the second layer is in general not very well resolved,

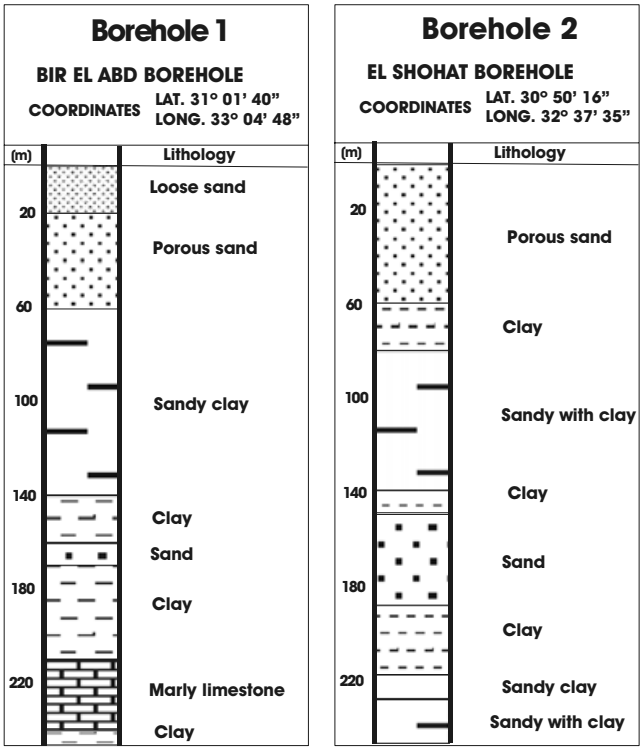

Figure 7. Description of the boreholes 1 and 2 (from Sultan & El Sorady 2001).

mainly due to the small number of data points sampling the last layer.

Resistivity-gravity joint inversion

An analysis of the Bouguer anomaly map shows that the structures in the survey area have a preferentially 3-D behaviour. Therefore, the interpretation based on 2-D models is necessarily incomplete and biased. However, the spacing between the VES profiles and the area covered by the resistivity survey are not adequate for a 3-D interpretation. It is believed that the results obtained from 3-D inversion would be more biased than those results from 2-D approach. The gravity and VES data along four profiles (Fig. 6a) were used in the joint inversion. Profiles 1, 2 and 3 run almost in the N–S direction, while the profile 4 runs in the NE–SW direction. The inversion parameters (initial temperature and weights) used when processing of profiles had the same values as those used in the synthetic example. Four-layer models were adopted for all profiles. The density values of the layers were, from top to bottom: 2000 kg m^{-3} (corresponding to sand), 2150 kg m^{-3} (water-bearing zone), 2300 kg m^{-3} (corresponding to the silt and silty sand and limestone partially filled by sea water) and 2670 kg m^{-3} for the bedrock (environment). The previous interpretation has showed that the main features of the VES can be in general, modelled by a three-layer earth. The use of a more layers model at some particular sites (for example VES-9, 11 and 14) would improve the fit between data and model response. However, the use of a different number of layers only at a few numbers of sites is not allowed by the current version of the code.

The models obtained by the joint inversion, together with some of the model responses for each profile are shown in Figs 8(a)–(d). The estimated resistivity distributions beneath each VES site are displayed in Table 4. The misfit between data and model response is, in general, good (Table 5).

The models suggest that the thickness of the first layer (ranging from 2 to 30 m) is thinner in the area of the profile 3. The resistivity of this layer ranges between 160 and 600 ohm-m. Low resistivity observed at VES-34 and VES-36 in profile 3 is due to local effects. The second layer shows resistivity values ranging from 1 to 8 ohm-m and variable thickness (ranging from 80 to 180 m), which is reflected in the geometry of its bottom. This interface represents the transition between the water-bearing zone and the layer contaminated by sea water. The third interface that represents the bottom of the third layer (mainly made up by limestone but with strong sea water infiltration in the upper part) is only constrained by gravity data. The feature of this interface is in accordance with the qualitative interpretation of the regional Bouguer map, suggesting that the bedrock is deeper northwards. The resistivity estimated for the third layer (<2 ohm-m) is only representative of the uppermost part of the layer. Because of the relative short AB spacing used in the VES, it is not possible to characterize the thickness of this low-resistivity layer. This is also the reason why the shape of the third interface is mainly controlled by the gravity data. Although the resistivity data does not constraint directly this interface, the results obtained from the synthetic example indicate that the improvement achieved in the uppermost interface's position, using the joint inversion, contributes definitively for a better resolution of the deeper interface. The bias originated by assuming a 2-D model approach for the gravity survey is evident when comparing the model misfit obtained from profiles 2 and 4. It is evident from Fig. 6 that the 3-D behaviour of the structures affects more than profile 4 than the 2.

5 CONCLUSIONS

The SA method was used in the implementation of an algorithm to jointly invert gravity and resistivity (VES) data in order to obtain the geometry of the density/resistivity interfaces and subsurface electrical resistivity distribution. The algorithm assumes the knowledge of the density distribution.

The results obtained from the inversions of a synthetic data set indicate a significant improvement of solutions when the joint inversion is used namely in the geometry of the uppermost interfaces. Although the geoelectrical equivalence problem cannot be completely solved by this method, it was observed, in the synthetic examples, a decrease in the ambiguity of the solutions. In conclusion, it was shown that the application of the proposed joint inversion method results in a more stable and reliable estimation of the model parameters.

The method was applied to gravity and resistivity data carried out in Sinai. The results obtained revealed the geometry of the water-bearing zone and of the bedrock interface, which are compatible with the geological information of the area. There are some limitations in the results presented in this work due to the 1-D approximation for the resistivity survey. The extension of the fundaments of the method to 2-D and 3-D models is straightforward. However, a code based on the SA method will be very time consuming and less effective for practical applications. A new algorithm, based on finite element method, is now in development and will be presented in a future work.

ACKNOWLEDGMENTS

This work was developed in the scope of the cooperation agreement between the Centro de Geofísica da Universidade de Lisboa

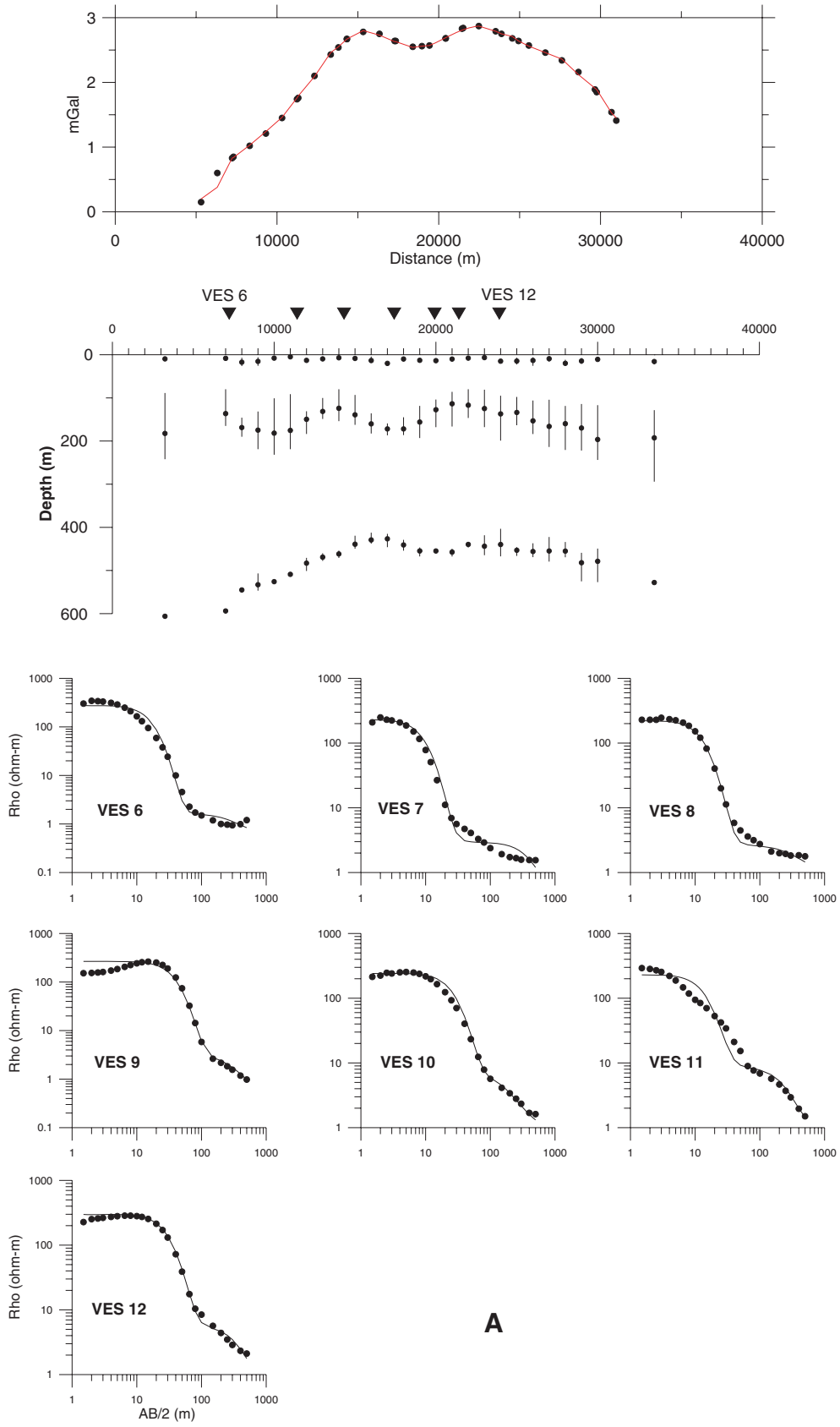

Figure 8. Results obtained from joint inversion of gravity and VES data carried out at the northwestern corner of Sinai (Egypt). The comparison between gravity data and model response is shown in top; the calculated model is shown in the centre and the comparison of the VES data and model response is in the bottom. (a), (b), (c) and (d) correspond to profiles 1, 2, 3 and 4, respectively.

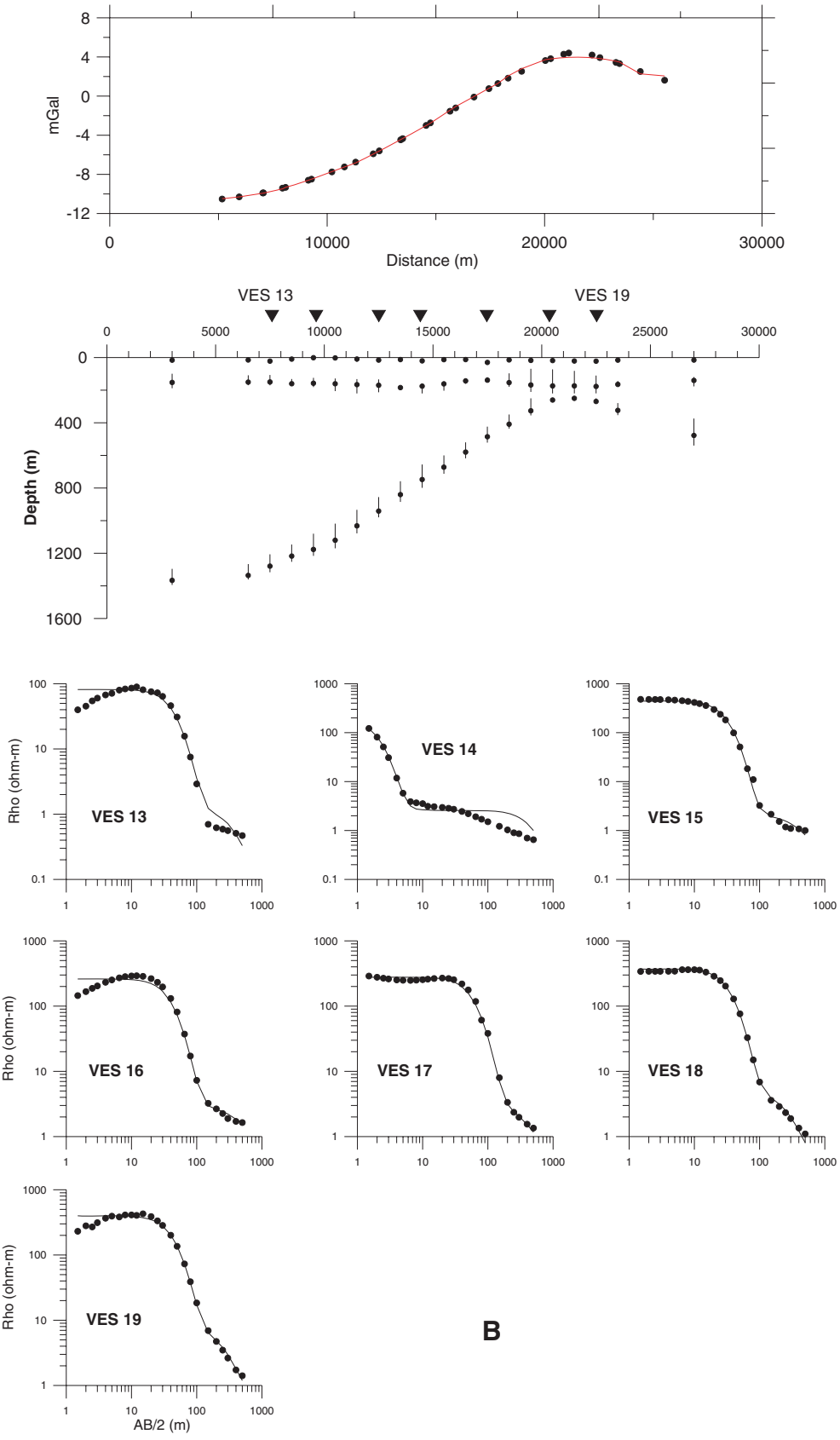

Figure 8. (*Continued.*)

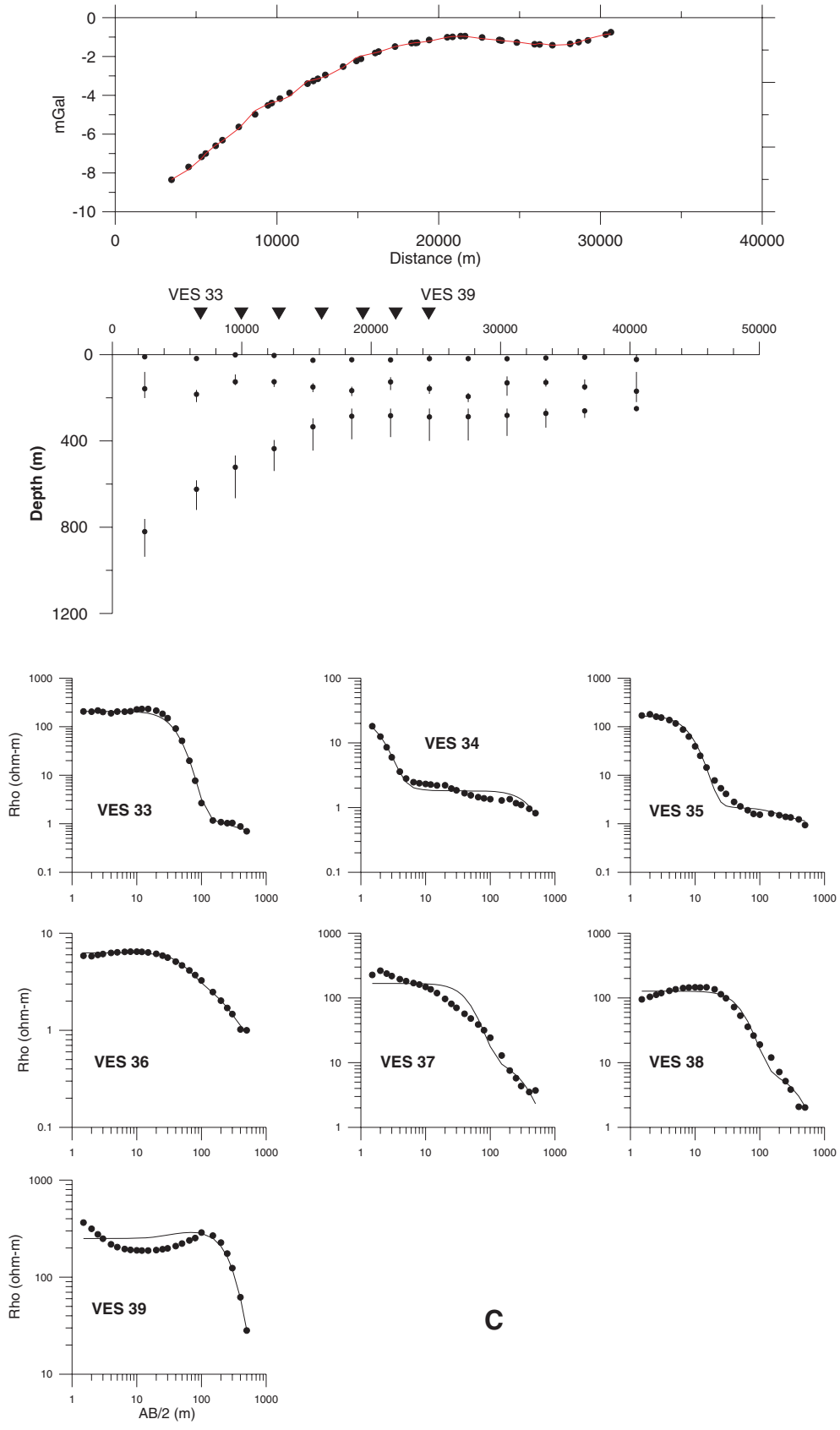

Figure 8. (*Continued.*)

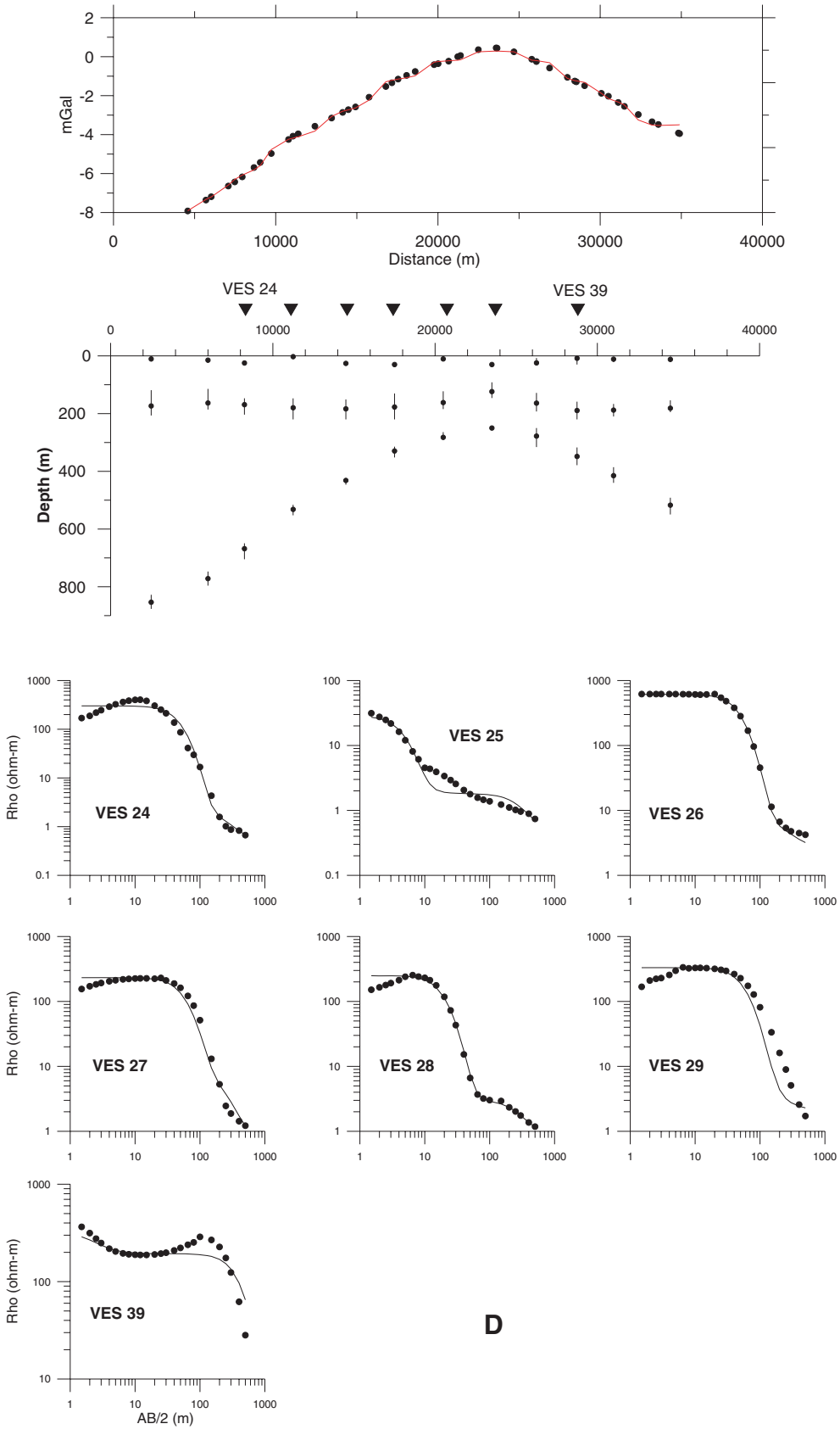

Figure 8. (*Continued.*)

Table 4. Averaged resistivity (and its maximum and minimum values calculated over six models) of the layers beneath each VES. Values in ohm-m. The values were estimated from joint inversion of gravity and resistivity data collected in Sinai.

Profile 1	VES-6	VES-7	VES-8	VES-9	VES-10	VES-11	VES-12
1st	**289.4**	**222.0**	**223.3**	**243.4**	**230.5**	**226.1**	**292.9**
layer	306.0–275.2	229.8–209.8	226.5–221.3	266.1–216.6	241.5–223.3	250.0–198.4	298.1–285.6
2nd	**1.4**	**2.8**	**2.9**	**2.5**	**5.1**	**7.9**	**6.5**
layer	1.6–1.3	2.8–2.7	3.7–2.4	2.7–2.5	5.6–4.5	8.6–6.8	7.3–5.1
3rd	**0.5**	**0.5**	**1.4**	**0.2**	**1.0**	**1.1**	**1.1**
layer	0.7–0.3	1.2–0.1	1.8–1.0	0.3–0.2	1.5–0.6	2.1–0.3	1.6–0.2
Profile 2	VES-13	VES-14	VES-15	VES-16	VES-17	VES-18	VES-19
1st	**81.9**	**180.0**	**443.9**	**267.1**	**271.4**	**348.7**	**399.4**
layer	88.8–79.4	181.6–177.3	467.3–404.5	285.3–245.7	281.6–261.8	363.0–341.7	400.0–397.1
2nd	**1.0**	**2.3**	**1.6**	**2.8**	**3.3**	**3.1**	**5.2**
layer	1.0–1.0	2.4–2.0	2.3–1.3	3.1–2.7	4.0–3.0	4.1–2.3	8.3–3.7
3rd	**0.3**	**0.1**	**0.1**	**0.7**	**0.9**	**0.4**	**1.1**
layer	0.3–0.2	0.1–0.1	0.2–0.1	0.9–0.6	1.0–0.6	1.8–0.1	1.4 –0.9
Profile 3	VES-33	VES-34	VES-35	VES-36	VES-37	VES-38	VES-39
1st	**232.2**	**24.8**	**163.3**	**6.3**	**160.8**	**134.5**	**282.6**
layer	237.0–218.9	25.6–24.5	167.7–159.4	6.4–6.3	165.2–157.5	136.1–131.5	380.5–250.0
2nd	**1.0**	**1.9**	**1.9**	**2.6**	**9.6**	**6.0**	**266.9**
layer	1.0–0.9	1.9–1.8	1.9–1.8	2.8–2.4	9.9–8.9	6.0–6.0	315.8–199.0
3rd	**0.4**	**0.6**	**0.7**	**0.5**	**1.0**	**1.9**	**0.9**
layer	0.5–0.3	0.8–0.5	0.7–0.6	0.5–0.4	1.3–0.8	2.0–1.7	1.5–0.1
Profile 4	VES-24	VES-25	VES-26	VES-27	VES-28	VES-29	VES-39
1st	**272.4**	**27.1**	**618.1**	**216.6**	**221.7**	**267.1**	**330.5**
layer	301.4–249.2	29.3–25.1	627.3–612.1	234.2–200.0	249.1–196.6	337.2–200.0	350.0–321.1
2nd	**1.5**	**1.7**	**5.9**	**4.6**	**2.7**	**6.0**	**164.2**
layer	2.0–1.1	1.8–1.5	6.0–5.7	6.0–3.0	2.8–2.5	6.0–5.9	207.4–160.0
3rd	**0.2**	**0.3**	**2.0**	**0.4**	**0.4**	**2.0**	**4.8**
layer	0.3–0.2	0.4–0.1	2.0–2.0	0.9–0.1	1.1–0.2	2.0–2.0	9.7–1.4

Table 5. Values of the objective function and misfit for the responses of the models shown in Figs 8(a)–(d).

Profile	ϕ	Gravity misfit (per cent)	VES misfit (per cent)
1	0.04	3.1	17
2	0.03	1.5	13
3	0.04	0.9	15
4	0.05	7.0	17

(Portugal) and the National Research Institute of Astronomy and Geophysics (Egypt). One of the authors (PR) was also funded by a grant of the Fundação para a Ciência e Tecnologia. Comments and suggestions from two anonymous reviewers greatly improved the first version of the paper.

REFERENCES

Barbosa, V.C., Silva, J.B.C. & Medeiros, W.E., 1999. Stable inversion of gravity anomalies of sedimentary basins with smooth basement relief and arbitrary density contrast variations, *Geophysics,* **64,** 754–764.

Blakely, R.J., 1995. *Potential theory in gravity and magnetic applications*, Cambridge University Press, USA, p. 441.

Bott, M.H.P., 1960. The use of rapid digital computing methods for gravity interpretation of a sedimentary basin, *Geophys. J. R. astr. Soc.,* **3,** 63–67.

Cordell, L. & Hederson, R.G., 1968. Iterative three-dimensional solution of gravity anomaly data using a digital computer, *Geophysics,* **54,** 621–631.

DeGroot-Hedlin, C. & Constable, S.C., 1990. Occam's inversion to generate smooth, two-dimensional models from magnetotelluric data, *Geophysics,* **55,** 1613–1624.

DeGroot-Hedlin, C. & Constable, S.C., 2004. Inversion of magnetotelluric data for 2D structure with sharp resistivity-contrast, *Geophysics,* **69**(1), 78–86, doi:10.11901.1649377.

Dey, A. & Morrison, H.F., 1979. Resistivity modelling for arbitrary shaped two-dimensional structures, *Geophys. Prospect.,* **27,** 106–136.

Dittmer, J. & Szymansky, J.E., 1995. The stochasti inversion of magnetics and resistivity data using the simulated annealing algorithm, *Geophys. Prospect.,* **43,** 397–416.

Dosso, S.E. & Oldenburg, D.W., 1991. Magnetotelluric appraisal using simulated annealing, *Geophys. J. Int,* **106,** 379–385.

Gallardo, L.A. & Meju, M.A., 2004. Joint two-dimensional DC resistivity and seismic travel time inversion with cross-gradients constraints, *J. geophys. Res.,* **109,** B03311, doi:10.1029/2003JB002716.

Geosoft Programs, 1994. *Geosoft mapping and processing system*, Geooft Inc., Toronto, Canada.

Grant, F.S. & West, G.F., 1965. *Interpretation theory in applied geophysics,* McGraw-Hill, New York, 584 pp.

Griffiths, D.H. & Barker, R.D., 1993. Two-dimensional resistivity imaging and modelling in areas of complex geology, *J. appl. Geophys.,* **29,** 211–226.

Haber, E. & Oldenburg, D., 1997. Joint inversion: a structural approach, *Inverse Problem,* **13,** 63–77.

Harinarayana, T., 1999. Combination of EM and DC measurements for upper crustal studies, *Surv. Geophys.,* **20**(3–4), 257–278.

IP1-D Program, 1993. *Programs st for 1-D VES data interpretation*, Dept. Geophysics, Geological Faculty, Mosco University, Russia.

Johansen, H.K., 1977. A man/computer interpretation system for resistivity soundings over a horizontally stratified earth, *Geophys. Prospect.,* **25,** 677–691.

Kirkpatrick, S., Gellat, C.D. & Vecchi, M.P., 1983. Optimization by simulated annealing, *Science,* **220,** 671–680.

Kis, M., 2002. Generalised Series Expansion (GSE) used in DC geoelectric-seismic joint inversion, *J. appl. Geophys.,* **50,** 401–416.

Koefoed, O., 1979. *Resistivity Sounding Measurements, Geosounding Principles I*, Elsevier, Amsterdam.

Last, B.J. & Kubik K., 1983. Compact gravity inversion, *Geophysics,* **48,** 713–721.

Li, Y. & Oldenburg, D.W., 1998. 3-D inversion of gravity data, *Geophysics,* **63**(1), 109–119.

Loke, M.H. & Barker, R.D., 1996. Practical techniques for 3-D resistivity surveys and data inversion, *Geophys. Prospect.,* **44,** 499–523.

Meju, M.A., 1996. Joint inversion of TEM and distorted MT soundings: some effective practical considerations, *Geophysics,* **61**(1), 56–65.

Metropolis, N., Rosenbluth, A., Rosenbluth, M., Teller, A. & Teller, E., 1953. Equation for state calculations by fast computing machines, *J. Chem. Phys.,* **21,** 1087–1092.

Oldenburg, D.W., 1974. The inversion and interpretation of gravity anomalies, *Geophysics,* **39,** 526–536.

Parasnis, D.S., 1986. *Principles of Applied Geophysics*, 4th edn, Chapman and Hall, London, p. 402.

Parker, R.L., 1973. The rapid calculation of potential anomalies, *Geophys. J. R. astr. Soc.,* **31,** 447–455.

Pessel, M. & Gibert, D., 2003. Multiscale electrical impedance tomography, *J. geophys. Res.,* **108**(B1), 2054, doi:10.1029/2001JB000233.

Patra, H.P. & Battacharya, P.K., 1966. Geophysical exploration for ground water around Digha in the coastal region of West Bengal, India, *Geoexploration,* **4,** 209–218.

Rothman, D.H., 1986. Automatic estimation of large residual statics corrections, *Geophysics,* **51,** 332–346.

Roy, L., Shaw, R.K. & Argwql, B.N.P., 2002. Inversion of gravity anomalies over sedimentary basins: application of genetic algorithm and simulated annealing. SEG Int'l Exposition and 72nd Annual Meeting, Salt Lake City, Utah.

Sasaki, Y., 1989. Two-dimensional joint inversion of magnetotelluric and dipole-dipole resistivity data, *Geophysics,* **54,** 254–262.

Sen, M.K. & Stoffa, P.L., 1995. *Global optimization methods in geophysical inversion*, Advances in Exploration Geophysics, Elsevier Science Publishers, Amsterdam.

Smith, T., Hoversten, M., Gasperikova, E. & Morrison, F., 1999. Sharp boundary inversion of 2D magnetotelluric data, *Geophys. Prospect.,* **47,** 469–486.

Sultan, S.A. & El Sorady, A.L., 2001. Geoelectric and gravity measurements for groundwater exploration and detection of structural elements at Romana area, Northwest of Sinai, Egypt., in Proceedings of the 6th Conf. Geology of Sinai for Development, Ismailia, 109–120.

Telford, W.M., Geldart, L.P., Sheriff, R.E. & Keys, D.A., 1978. *Applied Geophysics*, Cambridge University Press, Cambridge, p. 860.

Tikhonov, N. & Arsenin, V.Y., 1977. *Solution of Ill-Posed Problems*, V.H. Winston and Sons, Baltimore, MD.

Tsuboi, C., 1983. *Gravity*, 1st edn, George Allen & Unwin Ltd., London, p. 254.

Vozoff, K. & Jupp, D.L.B., 1975. Joint inversion of geophysical data, *Geophys. J. R. astr. Soc.,* **42,** 977–991.